Solubilization and characterization of the anthrax toxin pore in detergent micelles

Gregory Vernier,[1] Jie Wang,[1] Laura D. Jennings,[1] Jianjun Sun,[1] Audrey Fischer,[1] Likai Song,[2,3] and R. John Collier[1]*

[1]Department of Microbiology and Molecular Genetics, Harvard Medical School, 200 Longwood Ave., Boston, Massachusetts 02115

[2]Department of Medicine, Harvard Medical School, Boston, Massachusetts 02115

[3]Cancer Vaccine Center, Dana-Farber Cancer Institute, Boston, Massachusetts 02115

Received 1 June 2009; Accepted 25 June 2009
DOI: 10.1002/pro.199
Published online 16 July 2009 proteinscience.org

Abstract: Proteolytically activated Protective Antigen (PA) moiety of anthrax toxin self-associates to form a heptameric ring-shaped oligomer (the prepore). Acidic pH within the endosome converts the prepore to a pore that serves as a passageway for the toxin's enzymatic moieties to cross the endosomal membrane. Prepore is stable in solution under mildly basic conditions, and lowering the pH promotes a conformational transition to an insoluble pore-like state. *N*-tetradecylphosphocholine (FOS14) was the only detergent among 110 tested that prevented aggregation without dissociating the multimer into its constituent subunits. FOS14 maintained the heptamers as monodisperse, insertion-competent 440-kDa particles, which formed channels in planar phospholipid bilayers with the same unitary conductance and ability to translocate a model substrate protein as channels formed in the absence of detergent. Electron paramagnetic resonance analysis detected pore-like conformational changes within PA on solubilization with FOS14, and electron micrograph images of FOS14-solubilized pore showed an extended, mushroom-shaped structure. Circular dichroïsm measurements revealed an increase in α helix and a decrease in β structure in pore formation. Spectral changes caused by a deletion mutation support the hypothesis that the 2β2-2β3 loop transforms into the transmembrane segment of the β-barrel stem of the pore. Changes caused by selected point mutations indicate that the transition to α structure is dependent on residues of the luminal 2β11-2β12 loop that are known to affect pore formation. Stabilizing the PA pore in solution with FOS14 may facilitate further structural analysis and a more detailed understanding of the folding pathway by which the pore is formed.

Keywords: prepore-to-pore conversion; protein-detergent complex; conformational changes; biophysical characterization

Abbreviations: CD, circular dichroïsm; CDUB, circular dichroïsm universal buffer; CMC, critical micelle concentration; DLS, dynamic light scattering; DOGS-NTA-Ni, 1,2-dioleoyl-*sn*-glycero-3-{[*N*(5-amino-1-carboxypentyl) iminodiacetic acid]succinyl} (nickel salt); DOPC, 1,2-dioleoyl-*sn*-glycero-3-phosphocholine; DphPC, 1,2-diphytanoyl-sn-glycero-3-phosphocholine; EF, edema factor; EPR, electron paramagnetic resonance; FOS-PA, FOS14-solubilized PA pore; FOS14, N-tetradecylphosphocholine; LF, lethal factor; LF_N, residues 1-263 of LF; PA, protective antigen; UBB, universal bilayer buffer; VWA, von Willebrand factor A; WT, wild type.

Gregory Vernier and Jie Wang contributed equally to this work.

Grant sponsor: NIH; Grant numbers: AI022021, AI19807, AI057159; Grant sponsor: Gates Foundation (CAVD grant).

**Correspondence to:* R. John Collier, Department of Microbiology and Molecular Genetics, Harvard Medical School, 200 Longwood Ave., Boston, MA 02115. E-mail: jcollier@hms.harvard.edu

Introduction

Anthrax toxin is a major virulence factor of *Bacillus anthracis* and is believed to be responsible for many of the symptoms observed in infections caused by this organism. Besides its relevance to pathogenesis, this toxin has emerged in recent years as a tractable system to study protein translocation across membranes. The toxin is an ensemble of three large monomeric proteins. Two are enzymes that act on intracellular substrates within mammalian cells: Lethal Factor (LF; 90 kDa), a zinc protease, and Edema Factor (EF; 89 kDa), a calmodulin-dependant adenylyl cyclase. The third protein, Protective Antigen (PA_{83}; 83 kDa), is a receptor-binding and pore-forming transporter that conveys the two enzymic moieties into the cell and across the endosomal membrane to the cytosol.

After these three proteins are secreted by the vegetative bacteria, they interact in a sequence of events that begins with the binding of PA_{83} to a von Willerbrand A (VWA) domain of a cell-surface receptor.[1,2] PA_{83} is then cleaved by a cell-surface protease into 63-kDa (PA_{63}) and 20-kDa (PA_{20}) fragments. Dissociation of PA_{20} allows the self-association of PA_{63} to form a ring-shaped heptameric structure, the so-called prepore,[3,4] which can competitively bind up to three molecules of LF and/or EF.[5–9] The resulting complexes are internalized by endocytosis and trafficked to the acidic endosomal compartment, where the low pH induces a conformational rearrangement of the prepore to a membrane-spanning pore. The newly formed integral membrane protein mediates translocation of the unfolded catalytic components, EF and LF, across the membrane [Fig. 1(A)]. This transport through the PA_{63} pore is believed to occur via a Brownian ratchet mechanism and to be driven predominantly by the transmembrane pH gradient.[10] Within the cytosol, LF cleaves mitogen-activated protein kinase kinases[11] and EF converts ATP to cAMP,[12] leading to perturbation of various cellular functions and ultimately to symptoms of the infection.

Fractionation of trypsin-activated PA_{83} under mildly basic conditions (pH > 8) allows the prepore to be stably isolated in solution. The crystallographic structure of the prepore has been resolved both in the presence and absence of a VWA domain.[13] However, attempts to crystallize the pore have so far met with failure. The X-ray structure of the prepore and correlated biochemical and biophysical studies[14,15] suggest that the pore grossly resembles the α-hemolysin pore of *Staphylococcus aureus*,[16] a mushroom-shaped structure containing a globular cap and a 14-strand β-barrel stem spanning the membrane. This model received support from electrophysiological analysis of mutated forms of PA and has been confirmed in a recent study by electron microscopy, which yielded a ~25-Å-resolution structure.[17]

Domain 2 (residues 254–487) of PA undergoes a major conformational change during prepore-to-pore conversion [Fig. 1(B)], in which the 2β2-2β3 loop (residues 297–328) and the flanking β-strands (residues 275–350) are relocated to the base of the heptamer to form a 14-strand β-barrel stem.[13,18] There is also evidence for conformational changes elsewhere in domain 2, but details of these rearrangements and of the process of membrane insertion by the pore remain poorly defined.[19]

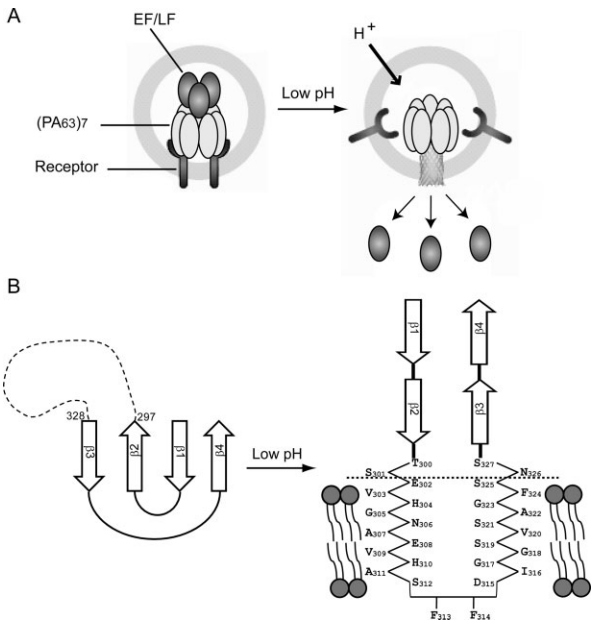

Figure 1. A: Schematic views of the prepore-to-pore conversion and translocation processes. For simplicity, the prepore is shown bound to only two receptors, although it is likely that every subunit is receptor-bound. EF/LF ligands are complexed to the prepore at the membrane surface, and the complexes are endocytosed. Acidification of the endosome triggers pore formation and translocation of the EF and LF components to the cytosol. Whether or not receptors remain bound to the pore is uncertain. B: pH-dependent membrane insertion of PA_{63}. At acidic pH, the Greek-key motif, strands 2β1 to 2β4 strands of domain 2, unfolds to form a β-hairpin. The seven β-hairpins interact to form a 14-strand β-barrel with the residues corresponding to the 2β2-2β3 loop spanning the membrane.[13,18] The dashed line demarcates the polypeptide segment deleted in the "loopless" mutant.

Obtaining atomic resolution structural information about the pore would represent a major breakthrough in the quest for a detailed understanding of how the structure is formed and how it functions. In the recent electron microscopy study that documented the pore's basic structure, GroEL was used as a molecular scaffold that interacted with the cap of the pore and minimized aggregation.[17] However, the GroEL-pore complexes were structurally inhomogeneous and retained a tendency to aggregate, thwarting attempts to obtain crystals. Use of detergents represents an alternative approach to inhibiting aggregation and sometimes allows crystallization of recalcitrant proteins. Detergents have also been extensively used for protein

folding and stability studies of membrane proteins, including β-barrel proteins, such as outer membrane proteins from gram-negative bacteria.[20–23] The choice of detergent is crucial in obtaining soluble, monodisperse, and functional proteins. Here, we report the identification of *N*-tetradecylphosphocholine (FOS14) as a detergent capable of solubilizing the PA_{63} pore in a form that retains the capacity to form ion-conductive channels in model membranes. We have characterized conversion of the prepore to the pore in the presence of FOS14 and described various properties of the detergent-solubilized pore.

Results

FOS14 prevents aggregation of the PA_{63} pore at acidic pH

We performed a screen for detergents that prevented aggregation of the PA_{63} pore at pH 5.5, using turbidity as a measure of aggregation. This pH value was chosen since it was shown to be optimal for PA pore formation and translocation in acidic endosomal compartments.[24,25] One hundred ten detergents frequently used for purification or crystallization of membrane proteins were tested.[26–29] Some of the results are shown in Figure 2(A). Only FOS14, a zwitterionic detergent, and SDS, an anionic detergent that causes dissociation of the prepore, were highly effective in preventing formation of turbidity when mixed with the prepore before acidification. Both FOS13 and FOS15 were inefficient in inhibiting aggregation, though each differs from FOS14 by only one methylene group.

In Figure 2(B), we show normalized turbidity at pH 5.5 as a function of the detergent/protein molar ratio (that is, the molar ratio of detergent to 63 kDa subunits). For all protein concentrations tested, no aggregation was observed at a detergent/protein molar ratio $\geq$500. However, at concentrations <1 mg/mL, both the cooperativity and the $FOS14/PA_{63}$ ratio at which turbidity was half-maximal decreased. This phenomenon may reflect the micellization effect on the protein–detergent interactions when the concentration of detergent is close to its CMC (0.12 m*M* in pure water for FOS14).[30] To avoid aggregation at low protein and detergent concentrations, we used a $FOS14/PA_{63}$ molar ratio of 1000, giving concentrations far above the CMC, in all subsequent experiments.

FOS14-solubilized PA_{63} pore is monodisperse

Monodispersity of FOS14-solubilized pore (FOS-PA) was demonstrated by dynamic light scattering and equilibrium analytical centrifugation. Light scattering measurements gave a distribution of intensities as a function of the apparent hydrodynamic radius (R_h) [Fig. 3(A)]. The R_h of the prepore (6.8 ± 0.7 nm) was consistent with a globular protein of 440 kDa, as calculated by the Omnisize software. FOS-PA samples at pH 5.5 showed two populations of particles: one with a small hydrodynamic radius (~4 nm), corresponding to free detergent micelles, and one with a larger radius, corresponding to protein-detergent complexes. The protein-detergent complexes showed a unimodal distribution, broader than that of the prepore. Five independent measurements gave an average R_h value of 17 ± 3 nm.

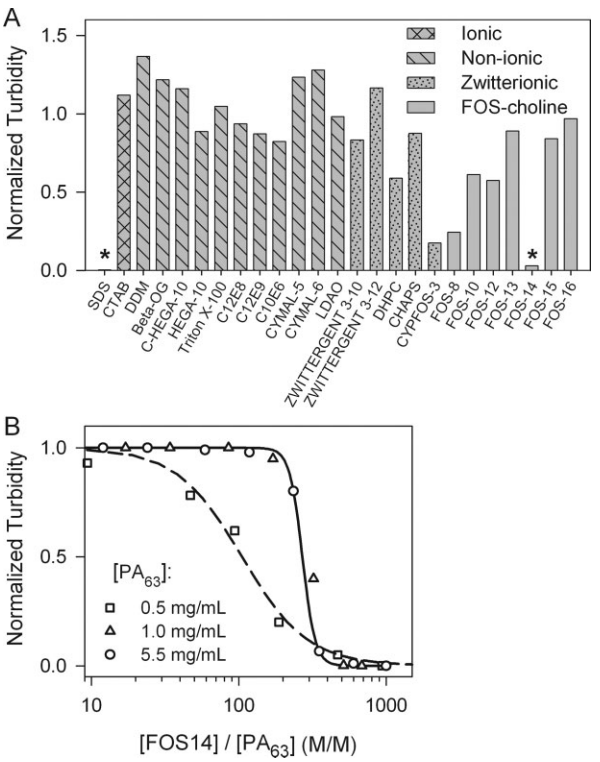

Figure 2. FOS14 prevents aggregation of PA_{63} at acidic pH. A: Detergents were screened at pH 5.5 with turbidity measurements taken at 340 nm. Data were normalized relative to a detergent-free control such that the OD value at pH 8.5 was defined as zero and the value at pH 5.5 as unity. A subset of the 110 detergents screened is shown. B: Turbidity as a function of the FOS14 to PA_{63} molar ratio for three protein concentrations. The continuous line corresponds to the best fit of the data. The $FOS14/PA_{63}$ ratio corresponding to half-maximal turbidity was 105 for 0.5 mg/mL and 270 for both 1 mg/mL and 5.5 mg/mL PA_{63}.

Equilibrium analytical ultracentrifugation measurements were made to determine the molecular weight of PA in detergent micelles. These measurements were performed in the presence of 5.5% D_2O to match the density of the solvent to that of the detergent. Under these conditions, the detergent made a negligible contribution to the overall sedimentation of the protein-detergent mixed micelles, allowing direct determination of the buoyant molecular mass of the protein. A representative sedimentation equilibrium data set is shown in Figure 3(B). Data collected at three concentrations and three speeds fit best to a single species with a calculated molecular mass of ~455 kDa. This value is within 2% of the expected mass for heptameric PA (444.3 kDa).

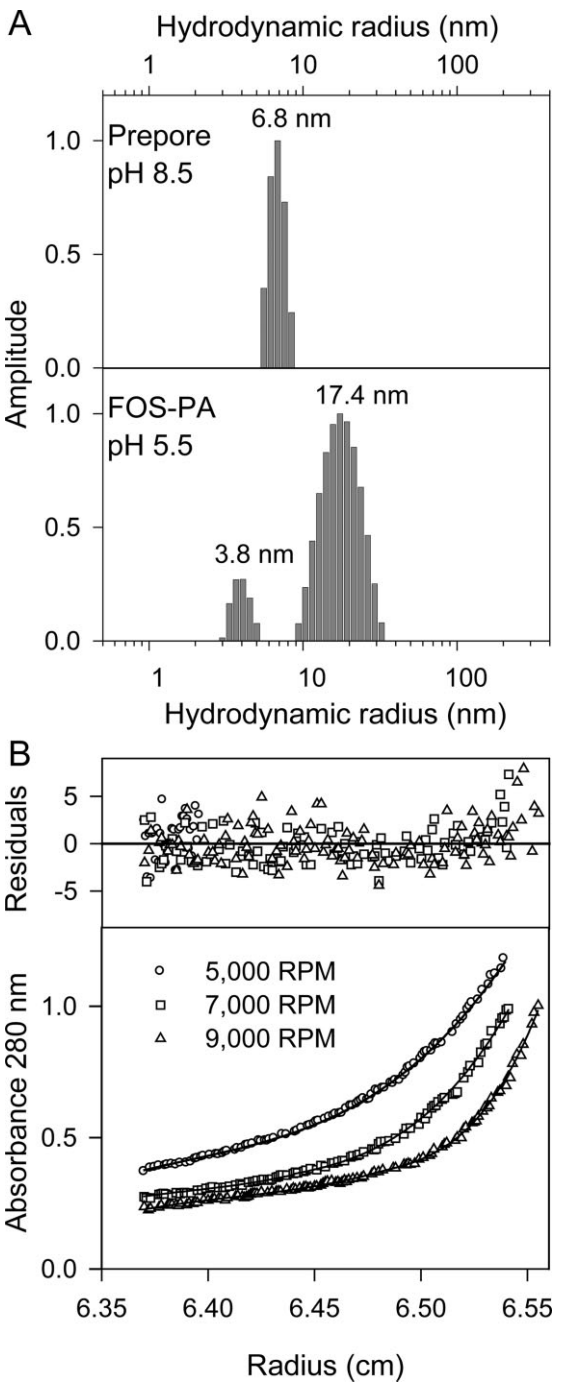

Figure 3. The PA pore in FOS14 is monodisperse and remains heptameric. A detergent to protein molar ratio of 1000 was used for all experiments. A: Hydrodynamic radius distribution from dynamic light scattering measurements of the prepore at pH 8.5 and FOS-PA at pH 5.5. The average hydrodynamic radius is shown for each population. B: Representative radial distributions from sedimentation equilibrium measurements performed at three speeds. D_2O was used to match the density of FOS14 for detergent-solubilized PA pore at pH 5.5 (protein concentration, 0.5 mg/mL). The residuals from the fit are shown in the upper panel and are uniformly distributed about the modal line. Data at three concentrations and three speeds gave a global fit of 455 kDa. The square root of the variance for the fit was 5.76×10^{-3}.

FOS14 solubilizes a pore-like state of PA

Having determined that FOS14 solubilizes a heptameric form of PA, we then used electron paramagnetic resonance (EPR) to probe the conformation of this heptameric species using site-directed spin labels (see Fig. 4). To this end, we first introduced a cysteine into the protein at one of two positions-residue 427, the site of the Phe clamp,[31] or 306, a lumen-facing residue within the membrane-spanning region of the pore[14] [Fig. 4(A,B)]. Next, we attached a nitroxide spin label (R1) to these cysteines and recorded the EPR spectra of the prepore, the pore, and FOS-PA. As the pore is membrane-inserted in vivo, we recorded the EPR spectra of this species inserted into liposomes. To facilitate this insertion, we utilized a previously published method in which Ni-chelating lipids are used to bind His-tagged variants of PA.[32] Membrane insertion/pore formation was initiated by dropping the pH to 6, and the EPR spectra were then recorded. For

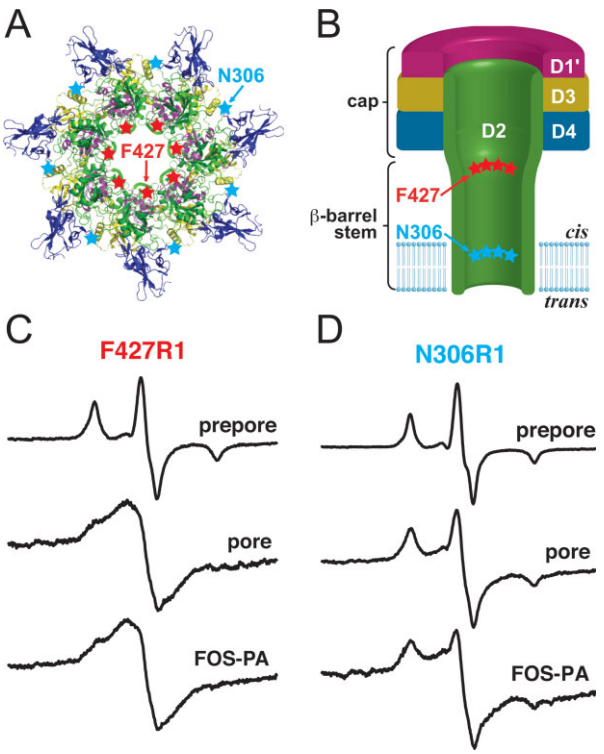

Figure 4. EPR analysis suggests FOS-PA adopts a pore-like conformation. A: The positions of F427 and N306 in the PA prepore crystal structure (PDB ID: 1TZO) are shown as red and blue stars, respectively. B: The putative positions of F427 and N306 in the PA pore are marked as in (A). Shown are the EPR spectra of (C) F427-spin-labeled and (D) N306-spin-labeled PA either in the prepore conformation (pH 8.5, bound to liposomes), the pore conformation (pH 6, inserted into liposomes), or solubilized by FOS14 at pH 6. All spectra were recorded at low temperature (233 K). Shown are representative spectra; the spectrum at each condition was recorded a minimum of three times, with little to no variation between trials.

consistency, prepore spectra were also recorded using His-tagged protein bound to Ni-chelating lipids with the pH held constant at 8.5.

We collected the EPR spectra of these PA variants at low temperature (233 K) to minimize spin label mobility and assess primarily spin-spin interactions (which are directly correlated to the distance between neighboring spin labels). We found that for PA spin labeled at residue 427, in agreement with the prepore crystal structure[13,18] and previously reported results,[31] the prepore showed weak spin–spin interaction, consistent with a distance between spin labels of ~20–25 Å, whereas the pore showed strong spin–spin interaction, indicating that the spin labels were less than 8 Å apart [Fig. 4(A–C)]. The EPR spectrum of FOS-PA F427R1 also showed strong spin–spin interaction, consistent with the idea that FOS14 solubilizes a pore-like state of PA [Fig. 4(C)]. In addition, the EPR spectrum of the prepore spin-labeled at residue 306 showed no detectable spin–spin interaction, consistent with the crystal structure in which these residues are ~50 Å apart [Fig. 4(A,D)].[13] However, as expected, the EPR spectrum of the N306R1 pore showed significantly more spin–spin interaction, corresponding to a spin–spin distance of less than 20 Å [Fig. 4(B,D)] and consistent with the formation of the membrane-spanning β-barrel. The FOS-PA N306R1 EPR spectrum also showed substantial spin-spin interaction [Fig. 4(D)], further supporting the idea that FOS14 stabilizes a pore-like conformation of PA. Collectively, the EPR data suggest that FOS14 solubilizes the PA pore.

Direct observation of detergent-solubilized PA_{63} pore

To directly address whether FOS14 solubilizes the pore conformation of PA, electron micrograph images of negatively stained prepore at pH 8.5 and FOS-PA at pH 5.5 were collected (see Fig. 5). Both samples showed homogeneous populations of particles, most being oriented with the sevenfold symmetry axis perpendicular to the plane of the microscope grid and a few with this axis parallel to the plane of the grid. The background was higher in the presence of the detergent [Fig. 5(A), right panel], but individual particles could be readily distinguished, and no amorphous aggregates were seen. We averaged images of top and side views of the particles from each sample independently. Consistent with a tightening of the structure observed in the recent electron microscopic study involving GroEL,[17,31] FOS-PA displayed a narrow cap (external diameter ~90 Å), relative to the prepore, and an extended stem, representing the 14-strand β-barrel tail [Fig. 5(B), lower right panel]. The shape of the prepore determined by particle averaging closely resembles the crystallographic structure of this oligomer, with an external diameter of ~120 Å.

FOS-PA forms functional pores in lipid bilayers

We found that FOS14-solubilized pore was capable of forming ion-conductive channels in a planar phospholipid bilayer system and furthermore that these channels promoted translocation of the model substrate, LF_N, the N-terminal PA binding domain of LF,[31] across the bilayer in response to a pH gradient. Pore formation of FOS-PA was observed with both compartments of the bilayer apparatus buffered at pH 8.5, and a transmembrane potential clamped at +20 mV (*cis*-positive). A small sample (0.1 μL) of prepore that had been incubated with FOS14 at pH 5.5 was added to the *cis* compartment (1 mL) and found to be highly active in pore formation, whereas neither prepore at pH 8.5 nor aggregated pore at pH 5.5 (formed by lowering the pH of a prepore-containing solution in the absence of FOS14) was able to form ion-conductive channels [Fig. 6(A)]. The observed conductance of the FOS-PA sample was dependent on the protein component of the sample, since FOS14 alone at 10 times the concentration used in the FOS-PA samples did not disturb the integrity of the membrane. Formation of ion channels by FOS14-solubilized protein at pH 8.5 is noteworthy, in that it shows that membrane insertion readily occurs at basic pH values if the pore is preformed in a nonaggregated state.

Since translocation of LF_N across black lipid membranes requires acidic conditions,[10,32,33] translocation experiments were initiated at symmetric pH 5.5. After channels were formed following addition of FOS-PA, we added LF_N and observed an almost complete blockage of current [Fig. 6(B)]. With the membrane potential held at +20 mV, we then raised the *trans* pH to 7.2 and observed a strong and rapid recovery of current, reflecting translocation through the PA pores. Indeed, the current was higher than at the time LF_N was added, due to the insertion of additional channels before the *trans* pH was raised. The conductance profiles observed with FOS-PA samples were similar to ones seen with detergent-free samples.[10,19] We also performed unitary conductance measurements under similar conditions on both PA and FOS-PA samples at symmetric pH 5.5. Channels formed by FOS-PA had the same unitary conductances (153 ± 4 pS) as channels formed by detergent-free samples (153 ± 2 pS) in 1*M* KCl [Fig. 6(C)]. Also, gel electrophoresis studies in the absence of SDS (data not shown) confirmed that FOS-PA was capable of binding LF_N.

Probing conformational changes by circular dichroïsm

CD spectra, carried out at a FOS14/PA_{63} ratio of 1000 showed a large change in secondary structure content in the presence of FOS14, relative to prepore (see Fig. 7). FOS-PA CD spectra displayed characteristics of an α/β-type protein with a predominant α-helical signal. We observed negative bands at 219–220 nm and 208–

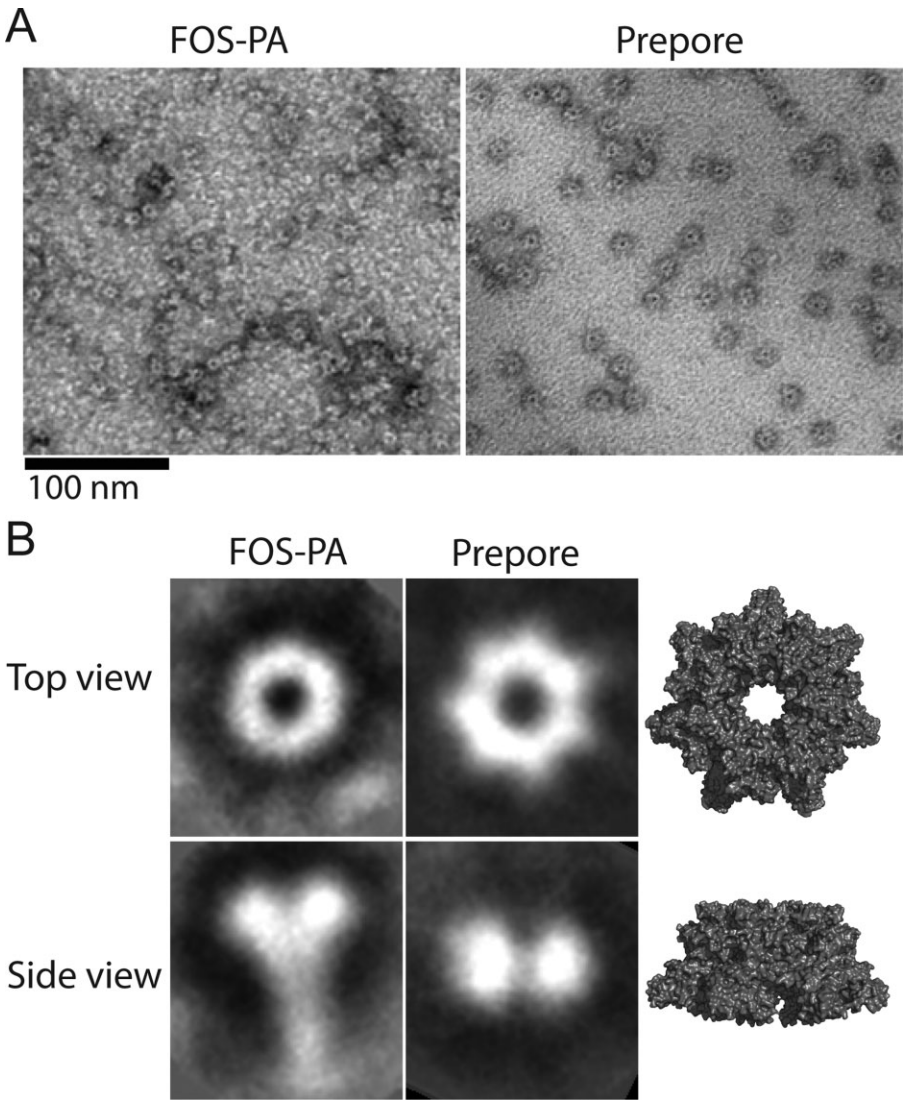

Figure 5. Negative-stain EM images of PA_{63} prepore and FOS14-solubilized pore. A: Left. FOS-PA at pH 5.5 with a detergent to protein molar ratio ~1000. Right, prepore. In the prepore micrograph, a homogeneous population of particles is observed, with most in aerial view. B: Class-averaged top- (upper panel) and side-views (lower panel) of FOS-PA (left) and prepore (right) particles. The top- and side-views of prepore were averaged from 157 and 136 independent particles, respectively. The top-view of FOS-PA was averaged from 68 independent particles and the side-view from 57 independent particles. Averaged images were obtained without imposing symmetry. Top- and side-views of the crystallographic structure of the prepore are also shown, for comparison.

210 nm, a positive band at 191–192 nm, and a crossover point at 200–201 nm. Ideal α-helical values are 222, 208, 190–195, and 205 nm, respectively.[34] Deconvolution of the FOS-PA CD spectrum yielded values of 33% α-helix, 20% β-strand, and 29% unordered structure. Spectral deconvolution of the prepore gave 15% α-helix, 28% β-strand, and 32% unordered structure, values close to those (16%, 27%, and 28%, respectively) calculated from the crystallographic structure of the prepore (PDB ID code 1TZO) with the DSSP algorithm.[35]

We monitored the kinetics of the changes in secondary structure when the prepore was converted to the pore in the presence of FOS14 by measuring the CD signal at 218 nm (inset, Fig. 7). Experiments were carried out at a high FOS14/PA_{63} ratio [FOS14/PA_{63} = 5000] to prevent protein aggregation that could occur when FOS14 and acidic buffer were added simultaneously. The excess detergent did not influence the final CD spectrum (data not shown). The rate of the conformational change at pH 5.5 was rapid, the transition being complete in less than 150 s ($k_1 = 8.1 \times 10^{-2}$ s^{-1}, $k_2 = 1.9 \times 10^{-2}$ s^{-1}).

CD spectra of FOS-PA prepared from selected mutated forms of PA were also recorded. One was the so-called "loopless" mutant, which lacks residues 302–325 of the 2β2-2β3 loop [Fig. 1(B)]. The heptameric prepore form of the loopless mutant was well-folded, as shown by its CD spectrum (data not shown). Although the absence of the 2β2-2β3 loop prevents

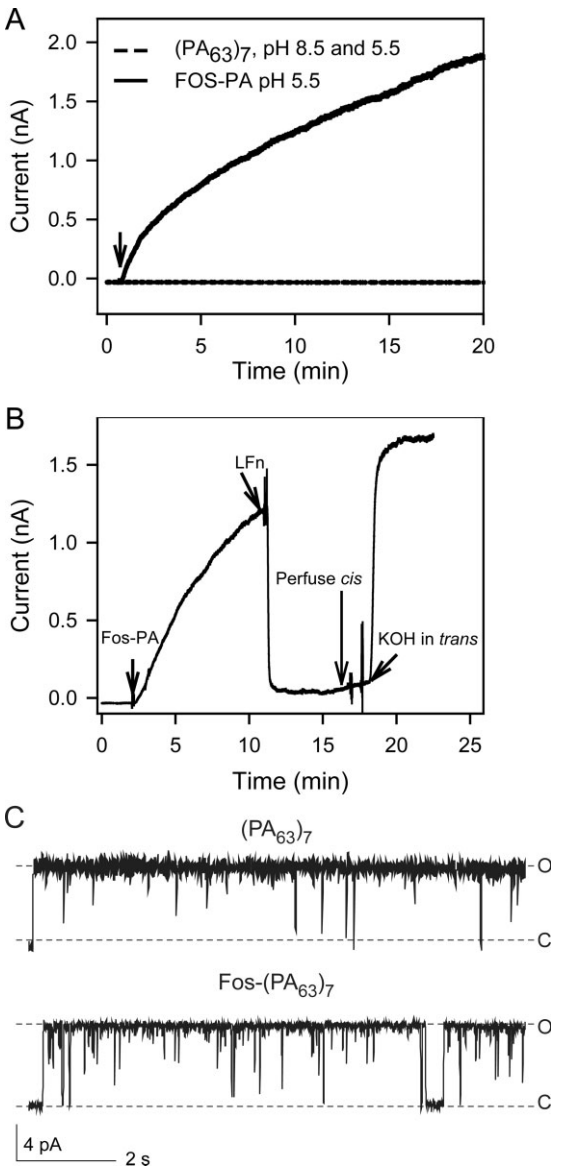

Figure 6. The FOS14-solubilized pore is functional in channel formation and translocation. A: Time course of the channel formation ($\Delta\Psi = +20$ mV); both chambers of the lipid bilayer apparatus were buffered at pH 8.5. The time of addition of the protein is indicated by the arrow. FOS-PA at pH 5.5 caused a robust increase in current, whereas prepore at pH 8.5 or prepore that had been pre-incubated at pH 5.5 caused no increase. B: Pore formation and LF_N translocation through PA_{63} channels formed with FOS-PA ($\Delta\Psi = +20$ mV, pH 5.5 in *cis* and *trans* chambers). Once the current reached ~1 nA, LF_N was added to the *cis* compartment and found to block the current. Unbound LF_N was removed by perfusion of the *cis* chamber. Adding KOH to the *trans* chamber triggered LF_N translocation. C: Representative single-channel currents of heptameric PA, with and without pre-incubation with FOS14, recorded at +50 mV in 1*M* KCl. C and O denote the closed and open states. The conductance value for detergent-free $PA_{63} = 153 \pm 2$ pS and that for FOS-PA $= 153 \pm 4$ pS.

insertion into membranes, the loopless mutant converts to an SDS-stable form below pH 8 and is believed to undergo basically the same conformational changes as the wild-type protein.[36] We found the CD spectrum of loopless FOS-PA at pH 5.5 to be similar to that of the wild type, but with a slightly lower content of secondary structure [Fig. 8(A)]. The difference spectrum between the two proteins, although small in magnitude, was typical of β-structure with a negative band at 216 nm, a red-shifted positive band, and a red-shifted crossover point relative to a typical α-helix [Fig. 8(B)]. The lower β-structure content of the loopless mutant is consistent with the hypothesis that the 2β2-2β3 loop forms the distal segment of the 14-strand β-barrel of the pore.

CD spectra of selected point mutants were also recorded. The prepore spectra of all of the mutated forms were essentially identical to that of the wild-type prepore, indicating native secondary structures in the pore precursors (Table I). FOS-PA spectra of the F427S and F427W mutants, both of which are almost identical to the wild-type protein in pore forming activity,[32] were essentially superimposable on the wild-type spectrum [Fig. 8(C) and Table I]. In contrast, FOS-PA spectra of the F427R and D425A variants, two mutations known to perturb pore formation,[19,32,39] were readily distinguishable from the wild-type [Fig. 8(D)]. Deconvolution analysis of the FOS-PA F427R and D425A CD spectra revealed lower α-helix content (21% and 24%, respectively) and a slightly higher β-sheet content (25% and 24%, respectively) relative to the FOS14-solubilized wild type pore (Table I).

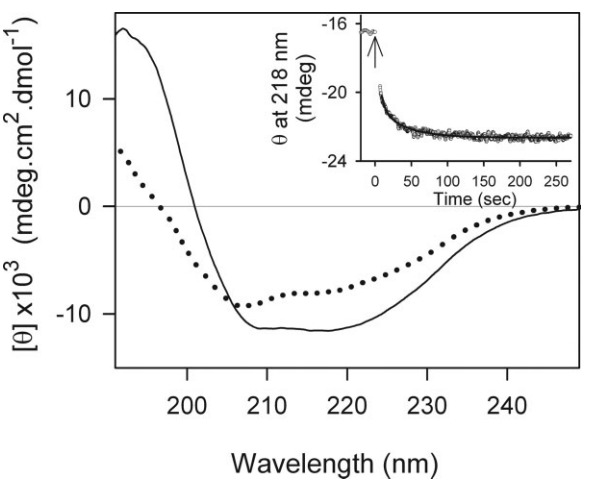

Figure 7. Circular dichroïsm spectra of the prepore and FOS-PA pore. CD spectra of detergent-solubilized PA_{63} at pH 5.5 (continuous line) and the prepore (dotted line) at pH 8.5; detergent to PA_{63} molar ratio = 1000. Inset: kinetics of the FOS14- and pH-induced conformational change. Ellipticity at 218 nm was monitored as a function of time after injection of the detergent/buffer mixture (black arrow) to give pH 5.5 and a FOS14/PA_{63} ratio of 5000. A burst phase was observed; the data following it were fit to a bi-exponential equation.

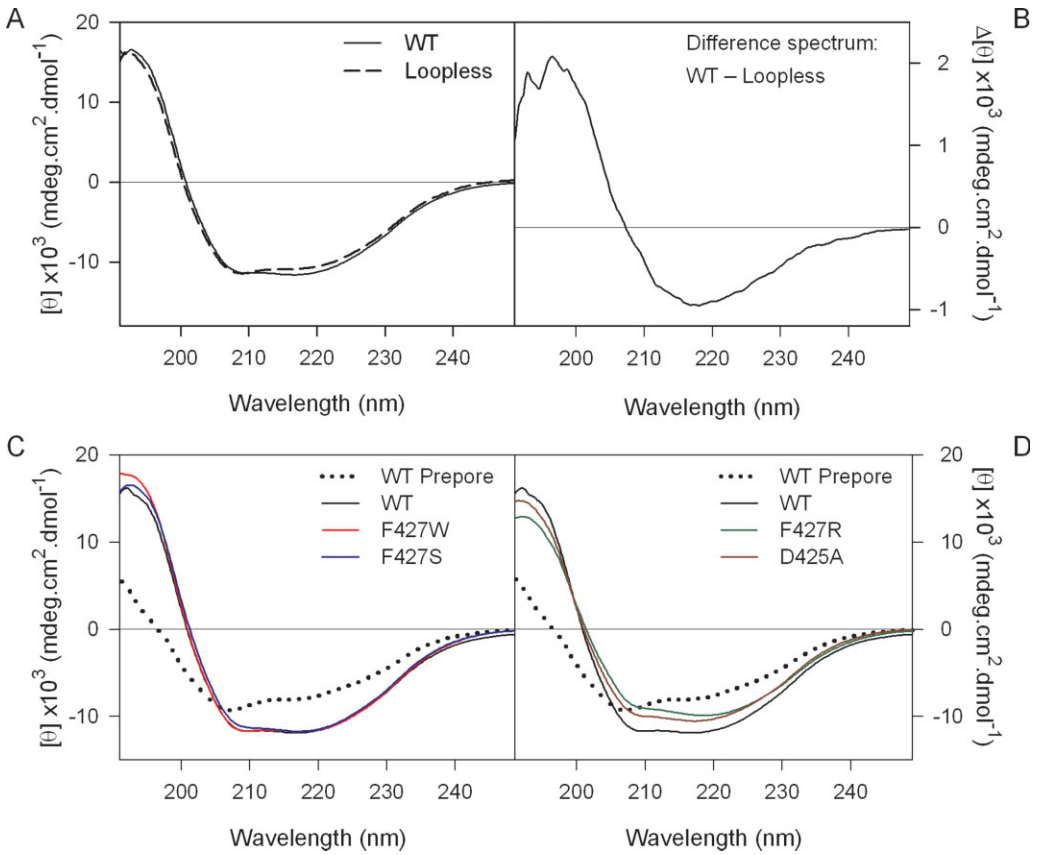

Figure 8. FOS14-induced conformational changes in various PA_{63} mutants. A: CD spectra of wild type (continuous line) and loopless mutant (dashed line) in the presence of FOS14 at pH 5.5. B: Difference spectra calculated from the CD spectra shown in A (wild type minus loopless). C: CD spectra of FOS-PA from wild type and two mutants that retain pore-forming activity, F427W and F427S. D: CD spectra of FOS-PA samples prepared from two mutants lacking pore-forming activity, F427R and D425A. In panels C and D, the CD spectrum of wild-type prepore is shown as a dotted line for comparison.

Table I. *Secondary Structure Content of Wild Type and Various Mutants of PA63 in the Presence and Absence of FOS14 Micelles*

PA sample	Pore formation	α helix (%)[a]	β strand (%)[a]	Random (%)[a]
$wtPA_{63}$	+			
Prepore (PDB 1TZO)		15.7[b]	27.1[b]	27.8[b]
Prepore		15.1	27.8	31.9
FOS-PA		32.7	20.0	28.9
F427S	+[c]			
Prepore		15.1	27.1	31.2
FOS-PA		32.0	20.4	29.0
F427W	+[c]			
Prepore		14.9	28.2	32.3
FOS-PA		29.7	21.5	28.4
Loopless	–[d]			
Prepore		14.5	26.8	32.9
FOS-PA		31.6	19.2	29.4
F427R	–[c]			
Prepore		14.2	28.1	32.4
FOS-PA		21.4	24.7	31.7
D425A	–[e]			
Prepore		15.3	28.5	32.1
FOS-PA		24.2	23.8	29.6

[a] The composition of the secondary structure of heptameric PA was analysed from CD spectra using DICHROWEB[37] and the CDSSTR algorithm.[38] The normalized root mean square deviation obtained for each analysis was ~0.05 or below.
[b] The secondary structure assignments of the crystallographic prepore (PDB ID code 1TZO) was done using the DSSP algorithm.[35]
[c,d,e] Respectively, from references 31, 36, 39.

Difference spectra using WT FOS-PA as a reference confirmed the absence of increased α-helix structure for the F427R and D425A mutants (data not shown).

Discussion

Obtaining a membrane protein in soluble form can be of major importance in facilitating biophysical and structural studies, and specifically could prove useful in obtaining two- or three-dimensional crystals of the anthrax toxin PA pore. We identified FOS14 as the only detergent among more than 100 tested that blocked aggregation of PA at pH 5.5 without dissociating the complex into its constituent subunits, as SDS is known to do. By various criteria, FOS14 maintained the structural and functional integrity of the PA_{63} heptamer at pH 5.5. Namely, the FOS14-PA complex at pH 5.5 was monodisperse and, as shown by analytical ultracentrifugation measurements, had the same particle weight as that calculated for heptameric PA_{63}. Comparison of the EPR spectra of spin-labeled PA shows that the FOS-PA spectra are unlike those of the prepore and nearly indistinguishable from spectra of the pore, strongly suggesting that FOS14 solubilizes a pore-like state of PA. This hypothesis is further supported by electron micrograph images; negatively stained samples of FOS-PA revealed a homogeneous population of mushroom-shaped particles closely resembling the 25 Å resolution pore structure reported recently.[17] Also, the detergent-protein complex formed ion-conductive channels in planar bilayers with the same properties as channels formed in the absence of detergent, as evidenced by both macroscopic and unitary conductance measurements. Channels formed with FOS14-solubilized PA both bound LF_N in a conductance-blocking manner and translocated this model protein substrate rapidly. Finally, mutations in PA known to affect the conformational change of the prepore to the pore also affected CD spectral properties of the FOS14-solubilized protein. Thus, by these criteria, the FOS14-solublized particles derived from the prepore under acidic conditions have the properties one would expect of a bona fide solublized functional pore.

Where on the pore structure does FOS14 bind? The distal, ~30 Å segment of the β-barrel stem of the pore, formed by domain 2, is believed to be the hydrophobic, membrane-spanning part of the pore and is likely to be the major site of interaction with FOS14 micelles. The turn region of the 2β2-2β3 loop has two Phe residues (F313 and F314) that are believed to generate a highly hydrophobic tip (with 14 Phe residues!), which may initiate membrane insertion and could well represent the primary site of FOS14 binding.

We have no indication that FOS14 binds to other sites on the pore. Hydrophobic patches forming part of the EF/LF binding site on domain 1 represent potential sites of interaction, but we found that LF_N bound to both FOS-PA in solution and to channels generated by FOS-PA in planar bilayers, suggesting little or no detergent binding at this site. Similarly, since FOS14 did not disrupt PA heptamerization, we have no evidence that domain 3, whose only known function involves mediating interactions between PA_{63} subunits, was perturbed by FOS14. We did not test the possible interaction of FOS14 with domain 4 by measuring binding of the prepore to the VWA domain of anthrax toxin receptor 2, because fluorescence and CD measurements showed that FOS14 caused a significant conformational alteration in the VWA domain (results not shown).

A major benefit of solubilizing the pore in detergent is the ability to monitor conformational changes by CD. Studies on membrane insertion and folding of integral β-barrel-forming proteins have revealed similar conformations in micelles and in liposomal membranes.[40–42] Members of the phosphocholine family of detergents were recently used for the solubilization and characterization of a functional membrane protein[43–46] and for the 3D determination of the human multidrug transporter ABCG2.[47] Moreover, phosphocholine detergents were found to be effective in refolding OmpX, an outer membrane protein with an eight-stranded β-barrel structure.[48] Structural differences have been observed for some membrane proteins between their native states in membranes and their detergent-solubilized states (e.g., the mitochondrial voltage-dependent anion-selective channel[49] and KcsA potassium channel[50]), tempering conclusions about the latter state for any protein-detergent complex.

There is strong evidence that prepore-to-pore conversion involves major conformational changes in domain 2. According to the current model, the 2β1, 2β2, 2β3, and 2β4 strands flanking the hydrophobic membrane-insertion loop (the 2β2-2β3 loop) are stripped out of the β-barrel core of this domain. The loop and flanking strands from each of the seven subunits adopt a β hairpin configuration, and the seven β-hairpins combine to form a 100-Å long, 14-strand β-barrel. Our CD data on WT and loopless FOS-PA support the hypothesis that the 2β2-2β3 loop adopts a β-hairpin configuration in the pore.

Despite the increase in β structure inherent in this loop-to-β-hairpin conversion, our CD measurements suggest a net decrease in β structure content, and a significant increase in α-helix content in FOS-PA relative to the prepore. This increase in α-helix content is consistent with results from infrared spectroscopy measurements on PA pore inserted into liposomal membranes, which yielded a value of 34% helix.[51] Our CD measurements on two PA variants with mutations in the solvent-exposed 2β10-2β11 loop (residues 421–431) of domain 2 indicate that the increase of helix content depends on residues within this loop. Thus, both D425A and F427R blocked the increase in helicity, while permitting an apparent increase in β structure. These mutations are known to block conversion of the prepore to the pore, as shown both by

susceptibility to dissociation by SDS and by inability to form ion-conductive channels in membranes.[32,39,52]

The effect on α-helix formation by these mutations suggests that helices may form in the lumen of the PA pore by conversion from the mobile 2β10-2β11 loop and perhaps other structural elements. In the pore conformation, the seven F427 residues of the PA heptamer are believed to form a clamp, the so-called the Phe clamp, which catalyzes polypeptide translocation.[31] The site-directed spin-labeling measurements presented here and elsewhere, along with other biochemical studies, have indicated that the F427 side chains are drawn into close proximity (<10 Å) during pore formation. Also, presumed interactions between the seven side chains at this position in various F427X mutants promoted prepore-to-pore conversion.[32] We suggest that one or more loops-including 2β10-2β11-of domain 2 may be involved in α-helix formation within the lumen of the PA pore during the conformational rearrangement of the prepore to the pore, facilitating appropriate contacts and the geometry of the Phe clamp.

Methods

Proteins

Expression and purification of recombinant PA, its mutants, and LF_N were performed as described.[32,33,36,39] The heptameric prepore form of PA_{63} was prepared from full length monomeric PA_{83} by trypsination, followed by anion-exchange chromatography.[36] The protein was stored in 20 m*M* Tris-HCl buffer pH 8.5 in the presence of 150 m*M* NaCl. Protein concentrations were determined using the calculated molar extinction coefficient at 280 nm (49,640 M^{-1} cm^{-1} for wild-type PA_{63} and its mutants, and 17,920 M^{-1} cm^{-1} for LF_N).

Detergent screening

To determine which detergents support solubilization of the pore, we screened 38 commonly used detergents, such as hexaethylene glycol monodecyl ether ($C_{10}E_6$), *n*-dodecyl-β-D-maltoside (DDM), FOS14, tetraethylene glycol monooctyl ether (C_8E_4), 3-[(3-cholamidopropyl)dimethylammonio]-1-propanesulfonate (CHAPS), lauryl dimethylamine oxide (LDAO), and 1,2-diheptamoyl-*sn*-glycero-3-phosphoryl choline (DHPC) (Anatrace, OH), together with 72 detergents provided by Hampton Research (CA). Some of the data are shown in Fig. 2(A). The prepore at 2 mg/mL was incubated for 1 h in the presence of each detergent at five times the critical micelle concentration (CMC) (final volume = 0.1 mL). Then, the pH was lowered to pH 5.5 by adding 0.1 equivalent volume of 1*M* acetate buffer at pH 5.5. A SpectraMax M2 plate reader (Molecular Devices, CA) was used to measure turbidity at 340 nm after a 1-h incubation. Measurements after 24 h of incubation gave identical results. For selected candidates, further turbidity measurements were performed over a protein concentration range from 0.5 to 5.5 mg/mL and various detergent concentrations. The turbidity was monitored at 340 or 600 nm, depending on the protein concentration, to achieve a maximum OD below 1.2. Titration curves were fitted using the Hill equation: $P = P_i + (P_f - P_i)/(1 + (K/X)^{nH})$, where P is the measured parameter (turbidity), P_f and P_i are the final and initial values, respectively, X is the $FOS14/PA_{63}$ molar ratio, K is the apparent dissociation constant, and nH is the Hill coefficient.

Sample preparation in the presence of FOS14

Unless otherwise mentioned, all experiments and incubations were performed at room temperature. FOS14-solubilized heptameric PA samples (FOS-PA) were prepared by overnight incubation of the prepore in the presence of FOS14 either in 20 m*M* Tris pH 8.5 and 150 m*M* NaCl, 20 m*M* Tris pH 8.5, and 400 m*M* NaCl (EPR buffer) for EPR experiments, or circular dichroïsm universal buffer (CDUB) for CD experiments. The pH was then lowered to pH 5.5–6.0 by the addition of 1*M* sodium acetate buffer pH 5.5, and the samples were incubated for 1 h prior to analytical measurements. pH values were verified before each measurement.

Dynamic light scattering

Dynamic light scattering (DLS) was performed at 25°C using 3 μg of protein mixture in a 12-μL holding cuvette on a Viscotek DLS device (TX), equipped with a single photon counting module. The solutions were subjected to scattering by monochromatic light (50 mW diode laser, 830 nm), the scattered light intensity was measured at an angle of 90° and data were analyzed by the Omnisize 3.0 software (Viscotek, TX) to obtain the hydrodynamic radius. We performed five independent measurements, each obtained as the mean of 20 counts. Samples were prepared at 0.25 mg/mL both in the absence (prepore, pH 8.5) and in the presence of FOS14 (FOS-PA, pH 5.5) with $[FOS14]/[PA_{63}] = 1000$.

Sedimentation equilibrium

Sedimentation equilibrium experiments were conducted at 4°C in an analytical ultracentrifuge (Optima XLA; Beckman Coulter). FOS-solubilized PA_{63} was prepared as described above with $[FOS14]/[PA_{63}] = 1000$. Three samples at 0.25, 0.5, and 0.75 mg/mL protein were loaded into a six-channel equilibrium centrifugation cell and spun at 3000, 5000, and 7000 rpm. Data were acquired as an average of two absorbance measurements at a nominal wavelength of 280 nm and a radial spacing of 0.001 cm. The partial specific volume and solution density were calculated using Sednterp v.1.09.[53] The partial specific volume of PA_{63} was calculated as 0.7322 mL/g, and the micelle partial

specific volume for FOS14 is reported to be 0.9876 mL/g.[54] Experiments were carried out at a solvent density equal to that of FOS14 to eliminate the contribution of the buoyant molecular mass of the protein-FOS14 complex.[55] The density-matched buffer contained 5.5% (v/v) of D_2O. Data collected at three concentrations and three speeds fit best to a single species model using the XL-I software package (Beckman Coulter).

Site-directed spin labeling

PA was spin-labeled at residue 427 or 306 by reaction of an introduced cysteine at these positions with a nitroxide spin label [(1-oxyl-2,2,5,5-tetramethyl-$\triangle^3$-pyrroline-3-methyl)methanethiosulfonate (MTSL), Toronto Research Chemicals], resulting in the attachment of the R1 side chain. Immediately before reaction with MTSL, monomeric $PAF427C_{83}$, $PAN306C_{83}$, or C-terminally His-tagged variants of these proteins[32] were incubated with 10 m*M* DTT for 30 min at room temperature. Buffer exchange into PBS, pH 7.2, was then performed using a G-25 Sephadex column, and MTSL was added at a 10× molar ratio. The reaction was allowed to proceed overnight at 4°C, after which time a 100× molar excess of 2-bromoacetamide (Sigma) was added and allowed to react for 30 min at room temperature to block any unreacted cysteines. Buffer exchange was again performed using a G-25 Sephadex column, and the labeling efficiency was assessed by EPR. All variants were found to be 70–85% spin labeled. Heptameric PA_{63} was then generated and purified from these spin-labeled PA_{83} variants by trypsination and anion exchange chromatography as described earlier.

EPR spectroscopy

The EPR spectra of the PA prepore and pore were recorded in the presence of liposomes. Briefly, 500 μL of ~20 mg/mL liposomes (containing 8% DOGS-NTA-Ni/92% DOPC, prepared in EPR buffer as described previously)[32] were mixed with 1.5 mg of C-terminally His-tagged PA F427R1 or N306R1 prepore, and the mixture was incubated at room temperature for 30 min. The mixture was then centrifuged in a Sorvall Biofuge Fresco tabletop centrifuge for 30 min at 13,000 rpm to pellet the liposomes along with any attached protein. The supernatant was removed, and the liposomes were resuspended in 1 mL of EPR buffer and centrifuged again to wash and remove any unbound protein. The pellet was resuspended in 100 μL of EPR buffer. 50 μL of this sample was retained and used to record the EPR spectra of the prepore, while 50 μL was transferred to another tube. To this sample, 10 μL of 1*M* acetate buffer, pH 5.5, was added to drop the pH to 6 (facilitating membrane insertion/pore formation). The FOS-PA EPR samples were prepared using non-His-tagged PA F427R1 and N306R1 as described above with $[FOS14]/[PA_{63}] = 1000$. To eliminate motional averaging of spin-spin interactions, all EPR spectra were recorded at low temperature (233 K) using glycerol as a cryoprotectant. Immediately before EPR analysis, the samples were mixed in a 1:1 ratio with 80% glycerol, so that the final composition contained, along with either liposomes or FOS14, 10 m*M* Tris, pH 8.5, 200 m*M* NaCl, 40% glycerol, and ~100 μM PA_{63}. The EPR spectra were then recorded on a Bruker EMX spectrometer at a microwave power of 2 mW sweeping the magnetic field from 3260 to 3460 G at a frequency of 9.45 GHz. To assess spin-spin distances, the EPR spectrum of each heptameric sample was compared to the corresponding spectrum of monomeric PA_{83} F427R1 or N306R1. The monomeric samples were prepared either bound to liposomes or in the presence of FOS14 in the same way as the heptameric samples, as described earlier.

Electron microscopy

Images of PA_{63} prepore (pH 8.5) and FOS-PA particles were generated by negative staining electron microscopy. Prepore and FOS-PA samples were prepared at 10 μg/mL in the presence of 0.2 m*M* FOS14 for the FOS-PA sample. Samples (12 μL) were applied to the carbon film on a glow-discharged EM grid, which was then washed by pH 8.5 buffer (20 m*M* Tris-HCl, pH 8.5) and floated on a small drop (5 μL) of stain solution (0.75% uranyl formate) for a few minutes and then blotted off. The sample was dried and examined under a Tecnai™ G^2 Spirit BioTWIN (FEI Company, OR) at 49,000× magnification. Particles were classified either as top or side-views and class-averaged using EMAN 1.7 software.[56]

Planar lipid bilayer experiments

FOS-PA samples were prepared with a detergent over PA_{63} molar ratio set to 1000. Planar lipid bilayers were painted across a 200-μm aperture in a Delrin cup (Warner Instruments, CT) by the brush technique.[57] Membrane was made from 3% diphytanoylphosphatidylcholine (Avanti Polar Lipids, AL, USA) in *n*-decane, and bilayer formation was monitored by capacitance. Once membranes were formed, 15 ng protein was added to the *cis* chamber, and conductance was recorded as described, with modifications.[58] Briefly, both *cis* and *trans* compartments were bathed in 1 mL pH 8.5 universal bilayer buffer (UBB: 100 m*M* KCl, 1 mM EDTA and 10 m*M* each of potassium oxalate, potassium phosphate and MES). $\Delta\psi$, the membrane potential (defined as $\Delta\psi = \psi_{cis} - \psi_{trans}$,), was set to +20 mV throughout the experiment. For translocase activity measurements, the pH of both compartments contained UBB at pH 5.5, since translocation of LF_N across black lipid membranes requires acidic conditions.[58,59] Once the PA channels were formed, 0.1 nmol of LF_N was added to the *cis* chamber, and blockage of PA channels was measured by monitoring the current. The *cis* compartment was

slowly perfused with a one-syringe system containing pH 5.5 UBB to remove unbound LF_N. Seven microliters of 2*M* KOH was added to the *trans* compartment to raise the pH to 7.2 to initiate translocation. The translocation was monitored by a current increase across the membrane. Both compartments were stirred continuously throughout the experiments.

Single-channel measurements were obtained under conditions similar to macroscopic current recordings using a 100 μm aperture. Membrane separated the *cis* and *trans* compartments containing symmetric solutions of 1*M* KCl, 10 m*M* MES at pH 5.5 over a range of positive potentials (*cis* positive). Increments of ~0.4 ng of either FOS-PA (pH 5.5) or prepore (pH 8.5) were added until a single channel was observed. Data were analyzed using Clampfit v. 10.0 software (Axon Instruments, Sunnyvale, CA), and Microsoft Excel. Analysis was performed on 10 s records. Single channel conductance was calculated from Gaussian fits to current amplitude histograms. Experiments were repeated three times each.

Steady-state circular dichroïsm spectroscopy

CD experiments were performed on a JASCO-815 spectropolarimeter (Jasco, Japan). An average of 10 scans was recorded in the far-UV between 190 and 250 nm at 20 nm/min, using 0.5 nm resolution steps and a bandwidth of 2 nm. Samples were prepared as described earlier in CDUB containing 5 m*M* Tris-HCl, pH 8.5, and 50 m*M* Na_2SO_4 which has an ionic strength similar to that of 150 m*M* NaCl, but gives a low signal in the far-UV. Spectra were recorded using a 0.1 mm path length and a PA_{63} concentration of 30 μ*M* in the presence and absence of 30 m*M* FOS14 ($[FOS14]/[PA_{63}] = 1000$) at pH 5.5. All spectra were baseline-corrected and the Savitzky–Golay smoothing algorithm was used with a window width of 5 in the Jasco spectra analysis software. Spectra were normalized to the mean residue molar ellipticity ([Θ]), given by: $[\Theta] = \theta(\lambda)/10 \times c \times l \times n$, where θ is the recorded ellipticity in millidegrees at wavelength λ, *c* is the concentration in mol/L, *l* is the pathlength of the cuvette in cm, and *n* is the number of residues. Spectra were analyzed using the online DICHROWEB[37] server and the CDSSTR deconvolution method.[38] Among other deconvolution algorithms, such as SELCON3,[60] CONTIN-LL,[61] VARSLC,[38] and K2D,[62] the CDSSTR algorithm gave the best normalized root mean square deviation (NRMSD) and the best correlation with secondary structure content of the prepore calculated from the crystallographic structure. NRMSD values were ~0.05 or below.

Time-resolved CD spectroscopy

Measurements were done in a 1-cm cuvette with constant stirring at room temperature. Fifty microliters of FOS14 at 100 m*M* were previously mixed with 50 μL of 1*M* acetate buffer at pH 5.1 to reach a final pH value of 5.5. The solution was then manually injected with a syringe into the cuvette containing 0.5 μ*M* of prepore in CDUB (final volume = 2 mL, pH 5.5). Injection and mixing took <10 s. A high detergent to PA_{63} molar ratio (5000) was used to minimize aggregation of the protein that may occur by concomitant injection of FOS14 and acidic buffers. The CD signal was monitored at 218 nm, and the spectrum was remeasured after the kinetics measurements.

Acknowledgments

We are grateful to Dr. Ellis Reinherz for his support and for helpful suggestions for modifications of the manuscript. Some of the proteins employed in the study were prepared in the Biomolecule Production Core of the New England Regional Center of Excellence, supported by NIH grant number AI057159. We thank Robin Ross and her staff for these services. One of us (RJC) holds equity in PharmAthene, Inc.

References

1. Bradley KA, Mogridge J, Mourez M, Collier RJ, Young JA (2001) Identification of the cellular receptor for anthrax toxin. Nature 414:225–229.
2. Scobie HM, Rainey GJ, Bradley KA, Young JA (2003) Human capillary morphogenesis protein 2 functions as an anthrax toxin receptor. Proc Natl Acad Sci USA 100: 5170–5174.
3. Molloy SS, Bresnahan PA, Leppla SH, Klimpel KR, Thomas G (1992) Human furin is a calcium-dependent serine endoprotease that recognizes the sequence Arg-X-X-Arg and efficiently cleaves anthrax toxin protective antigen. J Biol Chem 267:16396–16402.
4. Saab-Rincon G, Gualfetti PJ, Matthews CR (1996) Mutagenic and thermodynamic analyses of residual structure in the alpha subunit of tryptophan synthase. Biochemistry 35:1988–1994.
5. Cunningham K, Lacy DB, Mogridge J, Collier RJ (2002) Mapping the lethal factor and edema factor binding sites on oligomeric anthrax protective antigen. Proc Natl Acad Sci USA 99:7049–7053.
6. Lacy DB, Lin HC, Melnyk RA, Schueler-Furman O, Reither L, Cunningham K, Baker D, Collier RJ (2005) A model of anthrax toxin lethal factor bound to protective antigen. Proc Natl Acad Sci USA 102:16409–16414.
7. Lacy DB, Mourez M, Fouassier A, Collier RJ (2002) Mapping the anthrax protective antigen binding site on the lethal and edema factors. J Biol Chem 277:3006–3010.
8. Mogridge J, Cunningham K, Collier RJ (2002) Stoichiometry of anthrax toxin complexes. Biochemistry 41: 1079–1082.
9. Mogridge J, Cunningham K, Lacy DB, Mourez M, Collier RJ (2002) The lethal and edema factors of anthrax toxin bind only to oligomeric forms of the protective antigen. Proc Natl Acad Sci USA 99:7045–7048.
10. Krantz BA, Finkelstein A, Collier RJ (2006) Protein translocation through the anthrax toxin transmembrane pore is driven by a proton gradient. J Mol Biol 355:968–979.
11. Duesbery NS, Webb CP, Leppla SH, Gordon VM, Klimpel KR, Copeland TD, Ahn NG, Oskarsson MK, Fukasawa K, Paull KD, Vande Woude GF (1998) Proteolytic inactivation of MAP-kinase-kinase by anthrax lethal factor. Science 280:734–737.

12. Leppla SH (1982) Anthrax toxin edema factor: a bacterial adenylate cyclase that increases cyclic AMP concentrations of eukaryotic cells. Proc Natl Acad Sci USA 79:3162–3166.
13. Lacy DB, Wigelsworth DJ, Melnyk RA, Harrison SC, Collier RJ (2004) Structure of heptameric protective antigen bound to an anthrax toxin receptor: a role for receptor in pH-dependent pore formation. Proc Natl Acad Sci USA 101:13147–13151.
14. Benson EL, Huynh PD, Finkelstein A, Collier RJ (1998) Identification of residues lining the anthrax protective antigen channel. Biochemistry 37:3941–3948.
15. Nassi S, Collier RJ, Finkelstein A (2002) PA63 channel of anthrax toxin: an extended beta-barrel. Biochemistry 41: 1445–1450.
16. Song L, Hobaugh MR, Shustak C, Cheley S, Bayley H, Gouaux JE (1996) Structure of staphylococcal alpha-hemolysin, a heptameric transmembrane pore. Science 274: 1859–1866.
17. Katayama H, Janowiak BE, Brzozowski M, Juryck J, Falke S, Gogol EP, Collier RJ, Fisher MT (2008) GroEL as a molecular scaffold for structural analysis of the anthrax toxin pore. Nat Struct Mol Biol 15:754–760.
18. Petosa C, Collier RJ, Klimpel KR, Leppla SH, Liddington RC (1997) Crystal structure of the anthrax toxin protective antigen. Nature 385:833–838.
19. Melnyk RA, Collier RJ (2006) A loop network within the anthrax toxin pore positions the phenylalanine clamp in an active conformation. Proc Natl Acad Sci USA 103: 9802–9807.
20. Conlan S, Bayley H (2003) Folding of a monomeric porin, OmpG, in detergent solution. Biochemistry 42: 9453–9465.
21. Dornmair K, Kiefer H, Jahnig F (1990) Refolding of an integral membrane protein. OmpA of *Escherichia coli*. J Biol Chem 265:18907–18911.
22. Jansen C, Heutink M, Tommassen J, de Cock H (2000) The assembly pathway of outer membrane protein PhoE of *Escherichia coli*. Eur J Biochem 267:3792–3800.
23. Surrey T, Jahnig F (1995) Kinetics of folding and membrane insertion of a beta-barrel membrane protein. J Biol Chem 270:28199–28203.
24. Abrami L, Reig N, van der Goot FG (2005) Anthrax toxin: the long and winding road that leads to the kill. Trends Microbiol 13:72–78.
25. Young JA, Collier RJ (2007) Anthrax toxin: receptor binding, internalization, pore formation, and translocation. Annu Rev Biochem 76:243–265.
26. Blaauw M, Dekker N, Verheij HM, Kalk KH, Dijkstra BW (1995) Crystallization and preliminary X-ray analysis of outer membrane phospholipase A from *Escherichia coli*. FEBS Lett 373:10–12.
27. Buchanan SK, Smith BS, Venkatramani L, Xia D, Esser L, Palnitkar M, Chakraborty R, van der Helm D, Deisenhofer J (1999) Crystal structure of the outer membrane active transporter FepA from Escherichia coli. Nat Struct Biol 6:56–63.
28. Dutzler R, Wang YF, Rizkallah P, Rosenbusch JP, Schirmer T (1996) Crystal structures of various maltooligosaccharides bound to maltoporin reveal a specific sugar translocation pathway. Structure 4:127–134.
29. Hirsch A, Breed J, Saxena K, Richter OM, Ludwig B, Diederichs K, Welte W (1997) The structure of porin from *Paracoccus denitrificans* at 3.1 A resolution. FEBS Lett 404:208–210.
30. Nielsen AD, Arleth L, Westh P (2005) Analysis of protein-surfactant interactions--a titration calorimetric and fluorescence spectroscopic investigation of interactions between Humicola insolens cutinase and an anionic surfactant. Biochim Biophys Acta 1752:124–132.
31. Krantz BA, Melnyk RA, Zhang S, Juris SJ, Lacy DB, Wu Z, Finkelstein A, Collier RJ (2005) A phenylalanine clamp catalyzes protein translocation through the anthrax toxin pore. Science 309:777–781.
32. Sun J, Vernier G, Wigelsworth DJ, Collier RJ (2007) Insertion of anthrax protective antigen into liposomal membranes: effects of a receptor. J Biol Chem 282:1059–1065.
33. Sun J, Lang AE, Aktories K, Collier RJ (2008) Phenylalanine-427 of anthrax protective antigen functions in both pore formation and protein translocation. Proc Natl Acad Sci USA 105:4346–4351.
34. Fasman GD (1993) Distinguishing transmembrane helices from peripheral helices by circular dichroism. Biotechnol Appl Biochem 18 (Part 2):111–138.
35. Kabsch W, Sander C (1983) Dictionary of protein secondary structure: pattern recognition of hydrogen-bonded and geometrical features. Biopolymers 22:2577–2637.
36. Miller CJ, Elliott JL, Collier RJ (1999) Anthrax protective antigen: prepore-to-pore conversion. Biochemistry 38: 10432–10441.
37. Whitmore L, Wallace BA (2004) DICHROWEB, an online server for protein secondary structure analyses from circular dichroism spectroscopic data. Nucleic Acids Res 32: W668–W673.
38. Compton LA, Johnson WC, Jr. (1986) Analysis of protein circular dichroism spectra for secondary structure using a simple matrix multiplication. Anal Biochem 155:155–167.
39. Sellman BR, Nassi S, Collier RJ (2001) Point mutations in anthrax protective antigen that block translocation. J Biol Chem 276:8371–8376.
40. Kleinschmidt JH, Wiener MC, Tamm LK (1999) Outer membrane protein A of *E. coli* folds into detergent micelles, but not in the presence of monomeric detergent. Protein Sci 8:2065–2071.
41. Pocanschi CL, Apell HJ, Puntervoll P, Hogh B, Jensen HB, Welte W, Kleinschmidt JH (2006) The major outer membrane protein of Fusobacterium nucleatum (FomA) folds and inserts into lipid bilayers via parallel folding pathways. J Mol Biol 355:548–561.
42. Tamm LK, Hong H, Liang B (2004) Folding and assembly of beta-barrel membrane proteins. Biochim Biophys Acta 1666:250–263.
43. Cook BL, Ernberg KE, Chung H, Zhang S (2008) Study of a synthetic human olfactory receptor 17-4: expression and purification from an inducible mammalian cell line. PLoS ONE 3:e2920.
44. Newstead S, Kim H, von Heijne G, Iwata S, Drew D (2007) High-throughput fluorescent-based optimization of eukaryotic membrane protein overexpression and purification in *Saccharomyces cerevisiae*. Proc Natl Acad Sci USA 104:13936–13941.
45. West M, Park D, Dodd JR, Kistler J, Christie DL (2005) Purification and characterization of the creatine transporter expressed at high levels in HEK293 cells. Protein Expr Purif 41:393–401.
46. Yakata K, Hiroaki Y, Ishibashi K, Sohara E, Sasaki S, Mitsuoka K, Fujiyoshi Y (2007) Aquaporin-11 containing a divergent NPA motif has normal water channel activity. Biochim Biophys Acta 1768:688–693.
47. McDevitt CA, Collins RF, Conway M, Modok S, Storm J, Kerr ID, Ford RC, Callaghan R (2006) Purification and 3D structural analysis of oligomeric human multidrug transporter ABCG2. Structure 14:1623–1632.
48. Zhang Q, Horst R, Geralt M, Ma X, Hong WX, Finn MG, Stevens RC, Wuthrich K (2008) Microscale NMR screening of new detergents for membrane protein structural biology. J Am Chem Soc 130:7357–7363.
49. Shanmugavadivu B, Apell HJ, Meins T, Zeth K, Kleinschmidt JH (2007) Correct folding of the beta-barrel of the

human membrane protein VDAC requires a lipid bilayer. J Mol Biol 368:66–78.
50. Encinar JA, Molina ML, Poveda JA, Barrera FN, Renart ML, Fernandez AM, Gonzalez-Ros JM (2005) The influence of a membrane environment on the structure and stability of a prokaryotic potassium channel, KcsA. FEBS Lett 579:5199–5204.
51. Wang XM, Wattiez R, Mock M, Falmagne P, Ruysschaert JM, Cabiaux V (1997) Structure and interaction of PA63 and EF (edema toxin) of Bacillus anthracis with lipid membrane. Biochemistry 36:14906–14913.
52. Sellman BR, Mourez M, Collier RJ (2001) Dominant-negative mutants of a toxin subunit: an approach to therapy of anthrax. Science 292:695–697.
53. Laue TM, Shah, BD, Ridgeway TM, Pelletier SL. Computer-aided interpretation of analytical sedimentation data for proteins. In: Rowe A, Harding S, Horton JC, Eds. (1992) Analytical ultracentrifugation in biochemistry and polymer science. Cambridge: Royal Society of Chemistry. p. 90–125
54. Maslennikov I, Kefala G, Johnson C, Riek R, Choe S, Kwiatkowski W (2007) NMR spectroscopic and analytical ultracentrifuge analysis of membrane protein detergent complexes. BMC Struct Biol 7:74.
55. Tanford C, Reynolds JA (1976) Characterization of membrane proteins in detergent solutions. Biochim Biophys Acta 457:133–170.
56. Ludtke SJ, Baldwin PR, Chiu W (1999) EMAN: semiautomated software for high-resolution single-particle reconstructions. J Struct Biol 128:82–97.
57. Mueller P, Rudin DO, Tien HT, Wescott WC (1962) Reconstitution of cell membrane structure in vitro and its transformation into an excitable system. Nature 194: 979–980.
58. Zhang S, Udho E, Wu Z, Collier RJ, Finkelstein A (2004) Protein translocation through anthrax toxin channels formed in planar lipid bilayers. Biophys J 87:3842–3849.
59. Zhang S, Finkelstein A, Collier RJ (2004) Evidence that translocation of anthrax toxin's lethal factor is initiated by entry of its N terminus into the protective antigen channel. Proc Natl Acad Sci USA 101: 16756–16761.
60. Sreerama N, Woody RW (1993) A self-consistent method for the analysis of protein secondary structure from circular dichroism. Anal Biochem 209:32–44.
61. Provencher SW, Glockner J (1981) Estimation of globular protein secondary structure from circular dichroism. Biochemistry 20:33–37.
62. Andrade MA, Chacon P, Merelo JJ, Moran F (1993) Evaluation of secondary structure of proteins from UV circular dichroism spectra using an unsupervised learning neural network. Protein Eng 6:383–390.